



Article

# Quantum Channel Extreme Bandgap AlGaN HEMT

Michael Shur 1,\*, Grigory Simin 2, Kamal Hussain 2, Abdullah Mamun 2, MVS Chandrashekhar 2, and Asif Khan 2

- <sup>1</sup> Rensselaer Polytechnic Institute, Troy, NY, 12180, USA; shurm@rpi.edu
- <sup>2</sup> University of South Carolina, Columbia, SC 29208, USA
- \* Correspondence: shurm@rpi.edu.

**Abstract:** — An extreme bandgap Al<sub>0.64</sub>Ga<sub>0.36</sub>N quantum channel HEMT with Al<sub>0.87</sub>Ga<sub>0.13</sub>N top and back barriers grown by MOCVD over bulk AlN substrate demonstrated a critical breakdown field of 11.37 MV/cm, higher than 9.8 MV/cm expected for the channel Al<sub>0.64</sub>Ga<sub>0.36</sub>N material. We show that the fraction of this increase is due to the quantization of the 2D electron gas. The polarization field maintains electron quantization in the quantum channel even at low sheet densities in contrast to conventional HEMT designs. An additional increase in the breakdown field is due to quantum-enabled real space transfer of energetic electrons into high-Al barrier layers in high electric fields. These results show the advantages of quantum channel design for achieving record high breakdown voltages and enabling superior power HEMT devices.

Keywords: HEMT, AlGaN, quantization, breakdown field, mobility.

1. Introduction

Ever since their emergence in the 1990s and early 2000s [1, 2, 3, 4, 5, 6] GaN High Electron Mobility Transistors have demonstrated superior performance for high voltage [7, 8, 9, 10], high frequency [11, 12, 13, 14], high temperature [15, 16] operation, and excellent radiation hard potential [17, 18]. The prime reasons for their superiority for operation in extreme environments are a wide energy gap leading to a high breakdown voltage and polarization doping [19, 20, 21, 22] supporting large sheet electron densities in the HEMT channels. A high polar optical phonon energy in GaN (91.2 meV [23, 24, 25] compared to 35 meV for GaAs [26, 27, 28]) and screening of impurity scattering by a large electron density in the device channel ensure a high field effect mobility, especially in the on state, and lead to a low onresistance for long [29, 30, 31, 32, 33, 34, 35-37] and short channel devices.[38]. In this paper, we show that these advantages could be dramatically enhanced using the Quantum Channel HEMT (QC-HEMT) design. QC-HEMT incorporates a thin channel comparable sandwiched between the top and bottom wide bandgap barriers. Fig. 1 compares conventional HEMT and QC-HEMT designs.

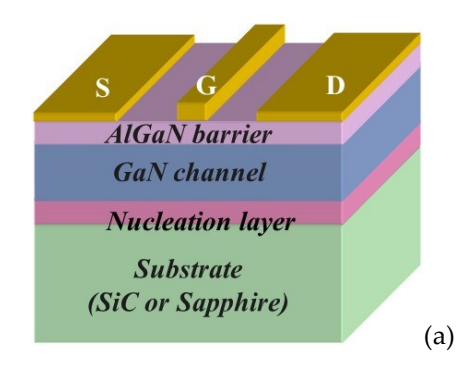
**Citation:** To be added by editorial staff during production.

Academic Editor: Firstname Lastname

Received: date Revised: date Accepted: date Published: date



Copyright: © 2024 by the authors. Submitted for possible open access publication under the terms and conditions of the Creative Commons Attribution (CC BY) license (https://creativecommons.org/license s/by/4.0/).



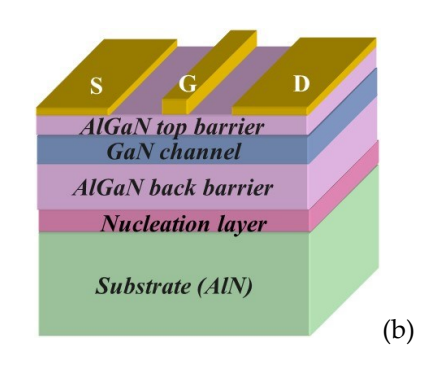


**Fig. 1.** Conventional (a) and QC-HEMT (b) designs. QC-HEMT in Fig. 1(b) can have GaN or AlGaN channel (GaN channel is shown).

In contrast to conventional GaN HEMT designs, the shape of the potential confining two-dimensional electron gas (2DEG) in QC-HEMT is determined by both the polarization field and bandgap discontinuities at the top and bottom barrier interface. Carrier confinement in the HEMT 2D electron gas (2DEG) channel affects most device performance parameters. Strong electron confinement reduces trapping and related gate- and drain lags, increases channel mobility, and helps achieve lower contact resistance. However, in conventional single heterojunction HEMTs, band diagrams flatten out at gate voltages close or below the threshold reducing or eliminating electron confinement. As we show in this work, in addition to maintaining confinement, the quantization of 2DEG in the QC design enables the effect that we call quantum real space transfer (QRST). QRST leads to achieving breakdown fields exceeding those predicted by the material properties of the device channel.

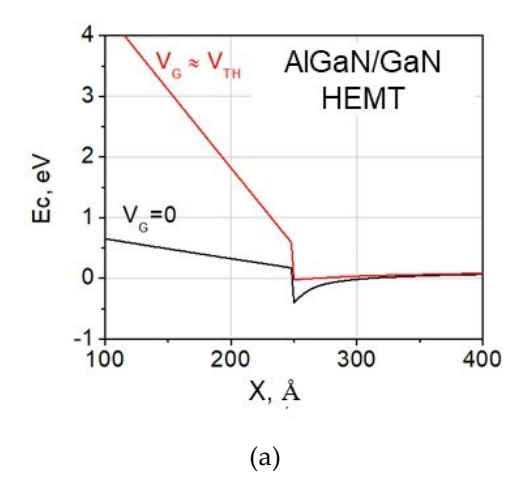
The QC HEMT advantages could be greatly enhanced using Extreme bandgap (EBG) semiconductors with bandgap energy exceeding  $4-5\,\mathrm{eV}$ , such as AlGaN with Al-fraction x>0.6. These devices show strong promise for achieving record high breakdown voltage, high-temperature operation, radiation hardness, and chemical stability. [ $^{39}$ ,  $^{40}$ ,  $^{41}$ ,  $^{42}$ ,  $^{43}$ ,  $^{44}$ ,  $^{45}$ ,  $^{46}$ ,  $^{47}$ ]

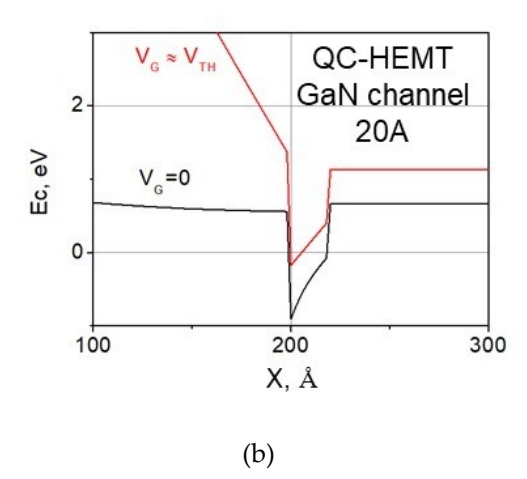
For high-power III-Nitride EBG devices, the choice of substrate has critical importance. Substrate lattice matching to device active layers is needed to avoid strain relaxation and defect generation. Bulk AlN is thus the best choice of substrate for high-Al Al-GaN devices [48, 49, 50, 51, 52, 53] and we employ it in our design. Bulk AlN substrate also has high thermal conductivity to provide efficient thermal management of high-power devices.

## 2. QC-HEMT design and key properties

## 2.1 Band diagrams and Energy states

Fig. 2 shows the energy band diagram of conventional AlGaN/GaN HEMT in comparison with QC HEMTs with different channel-barrier configurations. The band diagrams have been obtained using a 1D Poisson simulator by G. Shnider <sup>54</sup>





eV

Ec,

V<sub>o</sub>≈ V<sub>TH</sub>

 $V_{\overline{G}} = 0$ 

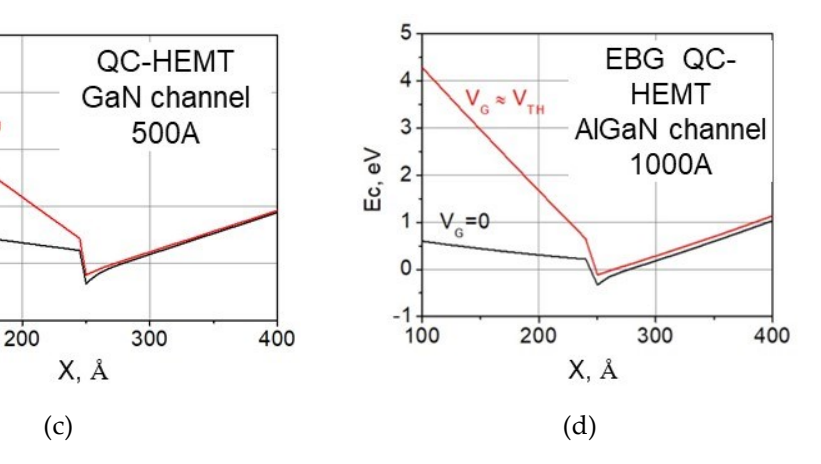


Fig. 2. Conduction energy band  $E_C$  diagrams of conventional HEMT and QC-HEMTs with different channel-barrier configuration as shown in the table 1 below.  $V_G$  and  $V_{TTH}$  are gate and threshold voltages correspondingly. The EBG HEMT in Fig.2(d) is included for comparison with experimental data discussed later in this paper.

Table 1

Details of device structures shown in Fig. 2

The position of ground state energy  $E_0$  above conduction band edge  $E_C$  was found using Eq. 2 below and from 1D Poisson simulations <sup>54</sup>

	Conventional HEMT	Thin channel QC HEMT	AlGaN/GaN/AlGaN QC-HEMT	EBG AlGaN QC-HEMT
Channel material	GaN	GaN	GaN	Al <sub>065</sub> Ga <sub>0.35</sub> N
Channel thickness	-	20 Å	500 Å	1000 Å
Al fraction in top/back barriers	25%	25% / 25%	25% / 25%	87% / 87%
Ground state $E_0$ location above $E_C$ at $V_{G} \approx V_{TH}$	-	0.54 eV	0.42 eV	0.15 eV

As compared to conventional HEMT Fig.2 (a) QC HEMT design Fig.2 (b-d) leads to two important results: first, the two-dimensional electron gas in the device channel is confined even at gate voltages close to the threshold and second, the ground state in the quantum well remains above the bottom of the conduction band in GaN.

As seen from Fig. 2, in conventional HEMT, the band diagram at the gate voltage  $V_G$  close to the threshold voltage  $V_{TH}$  flattens out and thus electrons are not confined in the vicinity of the barrier-channel interface. On the contrary, in QC-HEMT the band diagram maintains its profile in the entire  $V_G$  range from 0V to  $V_{TH}$ . Note that the triangular shape of Ec profile is maintained in a broad range of QC-HEMT channel thickness from 20A to 1000 A for devices examples shown in Fig. 2. This is due to the fact that the Ec profile is mainly determined by not only by conduction band discontinuity but also by electric field due to polarization charges at top and back barrier – channel interfaces. As long as the barrier and channel materials are not relaxed, this field maintains the QC-HEMT Ec profile.

It is important to point out that as long as the channel material is not relaxed and hence, the Ec profile maintains the triangular shape, the effective thickness of the channel is determined by the QW thickness at the level of ground energy state  $E_0$ , not by the total channel thickness. This is illustrated by an example Ec profile for 500A QC HEMT in Fig. 3a. At the gate voltage close to threshold, the ground state energy level  $E_0 \approx -0.017$  eV

below Fermi level. At this level, the effective width of the QW is around 10 Å. As we show below, in our experimental QC HEMT with 100 nm thick channel, the relaxation level is as low as 3.9%.

Better electron confinement in QC-HEMT in comparison with conventional HEMT is illustrated in Fig. 3b. For this comparison, we used an example of QC-HEMT with 500 Å thick channel. This channel thickness is much higher than the characteristic width of the 2DEG profile (around 30 Å). As described above, the confined shape of the 2DEG is due to strong polarization filed in the channel.

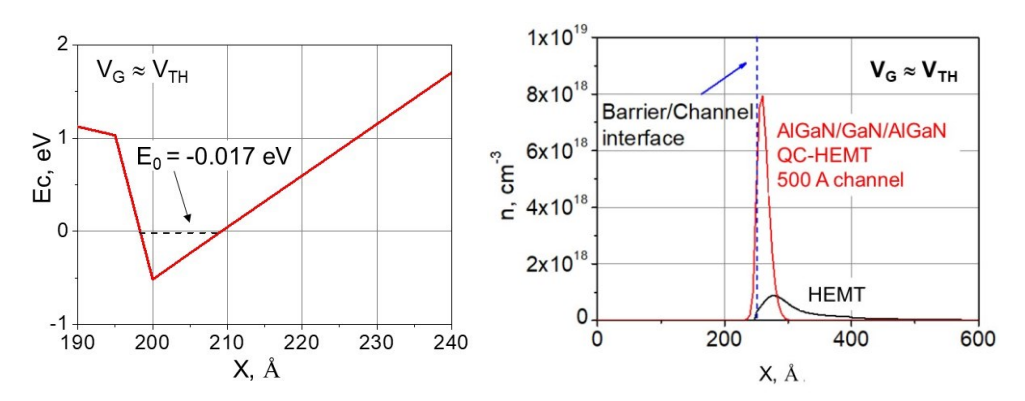


Fig. 3. Conduction band Ec profile (a) and electron density profile (b) at  $V_G \approx V_{TH}$  for QC-HEMT with 500Å thick GaN channel between 25%-Al top and back barriers. For comparison, Fig. 3b also shows electron density profile for conventional HEMT at  $V_G \approx V_{TH}$ 

The ground state energy E<sub>0</sub> can be estimated as <sup>55</sup>

$$E_o = \left(\frac{\hbar^2}{2m}\right)^{1/3} \left(\frac{3\pi}{2} q F_{eff}\right)^{2/3} \left(n_q + 3/4\right)^{2/3} \tag{1}$$

where  $n_q$  is the quantum number ( $n_q = 0$  for the ground state), and  $F_{eff}$  is the effective electric field in the channel. Our simulations show that, just like for Si MOSFETs [56] the effective electric field in the conventional HEMT is approximately

$$F_{eff} \approx \frac{F_i}{2} = \frac{qn_s}{2\epsilon\epsilon_0},\tag{2}$$

Here  $F_i$  is the electric field at the barrier-channel interface,  $n_s$  is the sheet electron density in the channel,  $\varepsilon_0$  is the dielectric permittivity of vacuum, and  $\varepsilon$  =8.9 is the GaN dielectric constant. Factor 2 in the denominator accounts for the band bending. For the QC HEMT

 $F_{eff} \approx F_s + \frac{F_i}{2}$ , where  $F_s$  is the polarization field that depends on the molar fractions of the

cladding layers and the QC thickness. We used a self-consistent solution of the Schrodinger-Poisson equation to estimate  $F_s = 10^8$  V/m. We have also found the ground energy states for QC HEMT using a 1D Poisson simulator by G. Snider <sup>54</sup> and obtained very close results (see Table 1).

Fig. 4 compares the dependencies of the ground state energy  $E_0$  above the bottom of the conduction band on the sheet carrier concentration  $n_s$  for the conventional HEMT (Fig. 2 (a)) and for the QC HEMT with a 20Å thick channel (Fig. 2(b)) generated using Eqs. (1-3).

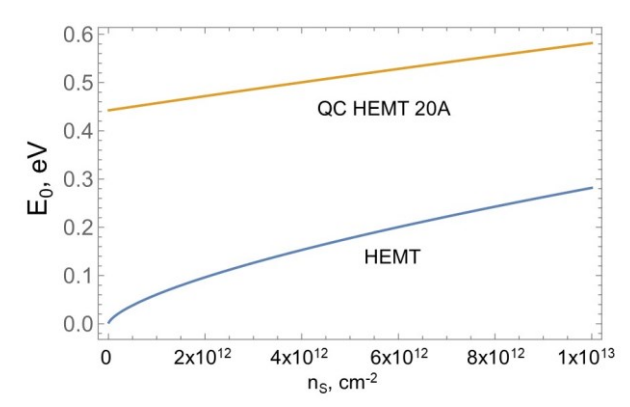


Fig. 4. Dependencies of the ground state energy  $E_0$  above the bottom of the conduction band on the sheet carrier concentration ns for the conventional HEMT and the QC HEMT with a 2 nm thick channel.

As seen, in conventional HEMT at gate voltage close to the threshold, ( $ns \Rightarrow 0$ ), the ground state energy practically coincides with the bottom of conduction band  $E_c$ . In contrast, in QC-HEMT, the ground state energy remains well above  $E_c$  in a broad range of 2DEG densities. This QC-HEMT feature makes an important impact on the device breakdown field.

### A. Breakdown field in QC-HEMT

As seen, the position of the lowest quantum state  $E_0$  in the quantum channel device remains practically constant even at  $n_s$  at the gate voltage close to the threshold. This is equivalent to the effective increase in the energy gap by  $E_0$ . Note that for the breakdown field consideration, the device parameters at the gate voltage close to the threshold are particularly important. The analysis presented in reference  $^{57}$  shows that the breakdown field,  $F_{CR}$ , is approximately proportional to  $E_0$ , consistent with the experimental data presented in  $^{58}$ . For QC-HEMT, the effective energy gap  $E_{Geff} = E_G + E_0$ . For the QC-HEMT example of Fig 2(b),  $E_G$  =3.39 eV,  $E_0$ =0.45 eV at gate voltage close to the threshold, and the resulting increase in an  $F_{BR}$  is around 36%.

The power dependence of FCR on EG can be understood by considering the ionization energy an ionizing electron must acquire  $F_{CR}\lambda = \alpha E_G$  to generate an electron-hole pair ( $\alpha$ >1). Its mean free path  $\lambda = v_{th}\tau \sim \tau/m^{1/2}$ . Here  $v_{th}\sim 1/m^{1/2}$  is the thermal velocity, m is the effective mass (inversely proportional to EG according to the Kane model). The scattering time  $\tau$  is inversely proportional to the optical phonon energy, which, in turn, is proportional to EG resulting in  $F_{CR}\sim E_G^{2.5}$ .

Strong electron confinement in QC-HEMT may lead to another important effect resulting in further  $F_{BR}$  increase. As shown in  $^{59}$  at high electron energies, real space transfer of hot electrons from the quantum well into the barrier should occur. Electron distribution in QC-HEMT in Fig. 3 shows that strong electron confinement leads to a significant fraction of electrons penetrating the top barrier.

Therefore, it is reasonable to expect that at a high electric field, a large fraction of the channel would experience quantum transfer to the top barrier. Since the top barrier is made of material with a larger bandgap (in our example, it is AlGaN with 65% Al), a further significant increase in the effective breakdown field  $F_{BR}$  is expected. This effect requires further theoretical and experimental studies.

# B. Electron mobility in QC-HEMT

Strong electric confinement in QC HEMT leads to a smaller 2DEG effective  $\Delta d$  thickness than it is for a conventional HEMT. The  $\Delta d$  could be estimated as the ratio of the ground state energy over the electric field at the heterointerface:

$$\Delta d \approx \frac{E_0}{qF_i} \tag{3}$$

Hence, bulk (volume) electron density for the same  $n_s$  value is higher in QC HEMT as compared to conventional HEMT. Fig. 5 shows the volume electron density as a function of  $n_s$  in conventional and QC HEMT calculated using Eqs. (1-3).

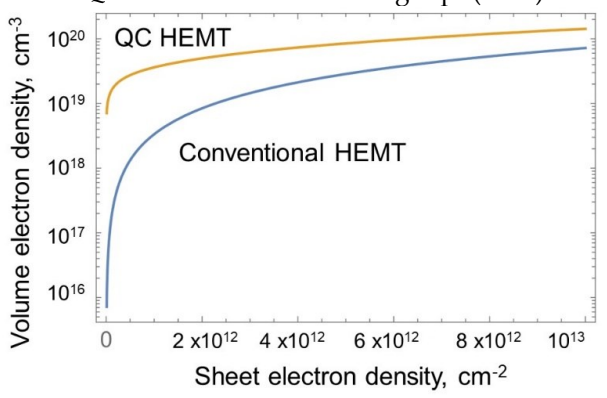


Fig. 5. 2DEG volume electron density as a function of n<sub>s</sub> in conventional and QC HEMTs

As seen, for conventional HEMT, volume electron density rapidly decreases as  $n_s$  decreases, i.e., as the gate bias approaches the threshold because the effective width of the 2DEG  $\Delta d$  in conventional HEMT rapidly increases as the gate bias approaches the threshold; 2DEG confinement nearly disappears. In QC HEMT, the volume electron density is a much slower function of  $n_s$ . A relative increase in volume density leads to better screening and less impurity scattering, hence to higher mobility. Fig. 6a illustrates this expected improvement extracted from the measured data. Experimental confirmation of mobility increase due to better confinement in double heterostructure (DH) HEMTs has been obtained earlier in 60. This data is shown in Fig. 6(b). The field effect mobility in III-Nitride HEMTs depends on many factors such as interface roughness, defect concentration, strain, alloy scattering, and dislocation density. However, strong scattering screening due to higher concentration should result in higher mobility in any HEMT. QC HEMT with a 2 nm thick channel exhibits nearly 10 times higher electron confinement than in the DH HEMT reported in 60.

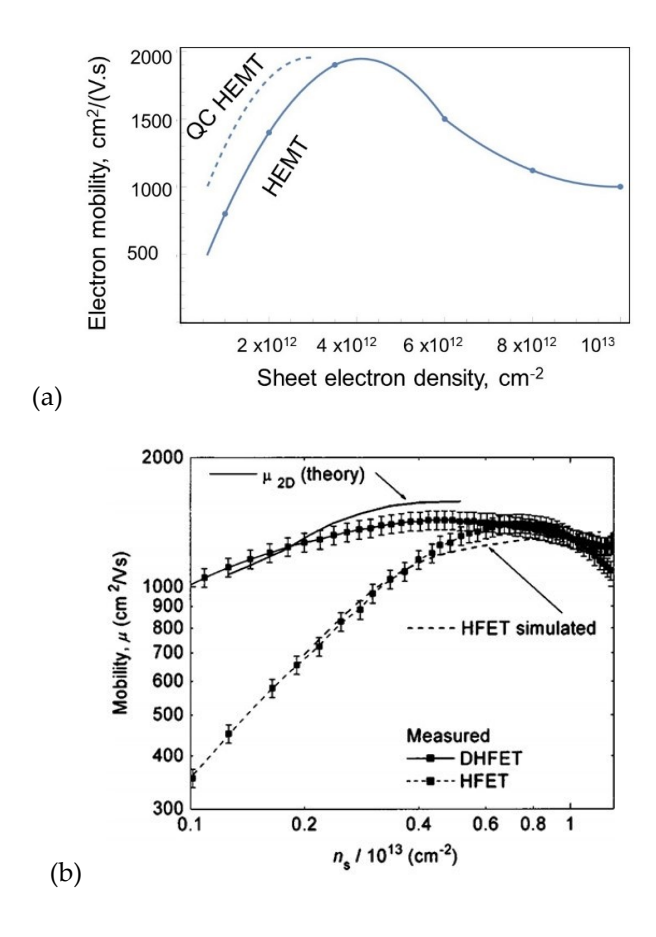


Fig. 6. (a) Expected mobility increase in QC HEMT; (b) experimentally observed mobility increase in double-heterostructure (DH) HEMT.

In thin channel devices with tight 2DEG distribution, there are also mechanisms lowering electron mobility, such as an increased phonon scattering <sup>61</sup> and alloy disorder scattering <sup>62</sup>

## 2. Experimental validation of QC HEMT breakdown field enhancement

### 2.1. Material growth and device fabrication

Pseudomorphic Al<sub>0.87</sub>Ga<sub>0.13</sub>N/Al<sub>0.64</sub>Ga<sub>0.36</sub>N/Al<sub>0.87</sub>Ga<sub>0.13</sub>N HEMTs with SiO<sub>2</sub> gate insulator were grown on a single crystal bulk AlN substrate low-pressure metalorganic-chemical vapor deposition (LP-MOCVD) <sup>39</sup>. The 2 × 2  $\mu$ m<sup>2</sup> AFM scan of the AlN substrate shows uniform parallel steps with root mean square (RMS) roughness ~0.089 nm. The LP-MOCVD growth was carried out at 1100 °C and 40 torr using trimethylaluminum (TMAl), trimethylgallium (TMGa), and ammonia (NH3) as the precursors. The epilayer structure and device design are shown in Fig. 7. The structure consisted of a 260 nm epitaxial AlN layer followed by a 140 nm Al<sub>0.87</sub>Ga<sub>0.13</sub>N back-barrier, a 100 nm Al<sub>0.64</sub>Ga<sub>0.36</sub>N channel layer, and a 23 nm thick Al<sub>0.87</sub>Ga<sub>0.13</sub>N barrier layer. To facilitate ohmic contact formation, the structure was capped with a 30 nm thick highly Si-doped reverse-graded Al<sub>x</sub>Ga<sub>1-x</sub>N (x = 0.87  $\rightarrow$  0.40) layer. The Reciprocal Space Mapping of (105) reflection shows the epilayer relaxation of 3.9% (Fig. 7b). More details can be found in <sup>39</sup>. Note that low relaxation level in the material supports the assumption of triangular conduction band profile in QC HEMT.

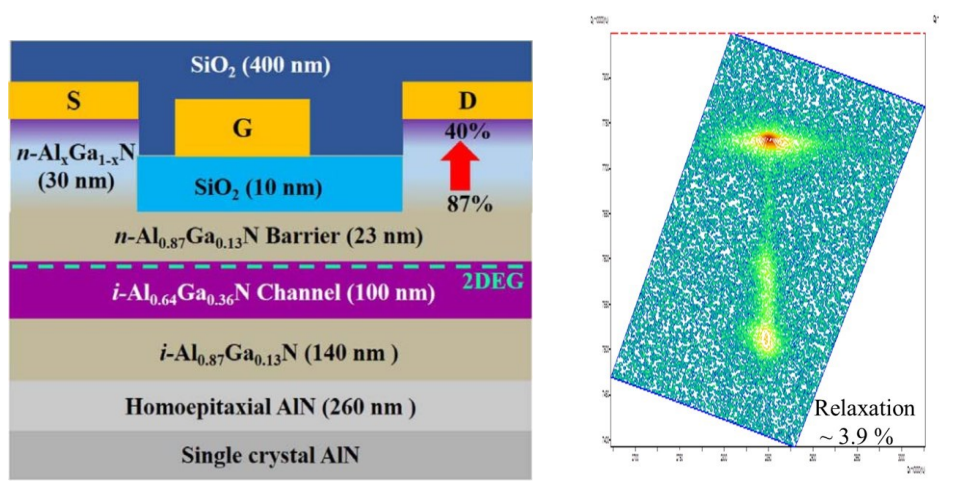


**Fig. 7.** Schematic cross-section (a) and Reciprocal Space Mapping of epilayer structure (b) of Al<sub>0.64</sub>Ga<sub>0.36</sub>N channel insulated-gate *E<sub>BG</sub>* HEMT <sup>39,40</sup>.

The device fabrication began with mesa isolation using inductively coupled plasma reactive ion etching (ICP-RIE). A Zr/Al/Mo/Au metal stack was deposited by electron beam evaporation for the source/drain contacts followed by rapid thermal annealing at 950 °C for 30 s. Then an ICP-RIE etch was used to remove the reverse-graded layer from the access region, and 10 nm SiO<sub>2</sub> was deposited as the gate oxide. Next, the gate and probe metal stacks were deposited consisting of Ni/Au (100/ 200 nm) and Ti/Ni/Au (500/700/1500 Å), respectively. Finally, the devices were capped with a 400 nm thick SiO<sub>2</sub> film to prevent surface flashover. The fabricated devices had a gate length  $L_G$  = 1.5 µm, source-gate spacing  $L_{GS}$  = 0.65 µm, various gate-drain spacing, and width W = 50 µm

The average on-wafer 2DEG sheet resistance measured using the Lehighton rf-mapping system was  $R_{SH}$  = 2400 Ohm/sq. Using the transfer length method (TLM) we obtained contact resistance  $R_C$  = 4.3 Ohm.mm and  $R_{SH}$  = 2400 Ohm/sq in close agreement with onwafer mapping. Electron mobility of 130 cm<sup>2</sup>V<sup>-1</sup>s<sup>-1</sup> at zero gate bias was extracted from C-V and transconductance measurements following the procedure described in <sup>29</sup> On-re-

sistance extracted from the device I-V was found to be 25  $\Omega$ .mm at V<sub>G</sub> = +2 V.

2.2 Electrical Characterization

We then measured a two-terminal breakdown voltage between the gate and source electrodes with  $L_{GS}$  = 0.65 µm spacing. Electrode spacing was verified using SEM imaging. We kept short electrode spacing to reduce electric field non-uniformity and prevent surface flashover. Fig. 8 shows the current-voltage characteristic for breakdown measurements. From the measured breakdown voltage  $V_{BD}$  =739 V, the average electric field at breakdown  $F_{BD}$  = 11.37 MV/cm was found. Drain current and transconductance I-V characteristics for EBG HEMT are shown in Fig. 9 <sup>40</sup>.

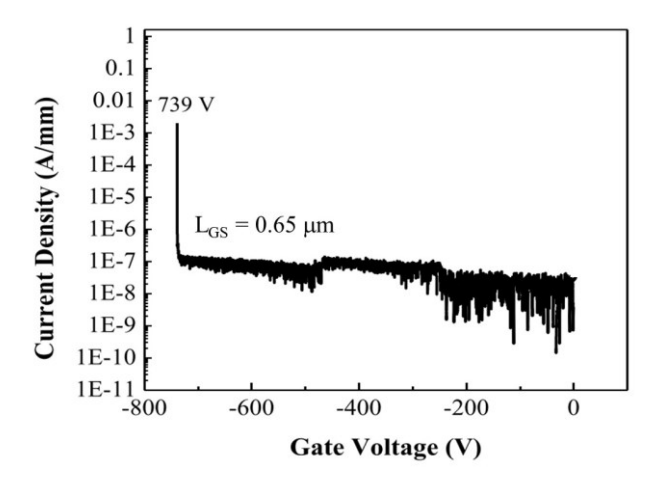


Fig. 8. EBG HEMT breakdown current-voltage characteristics [1].

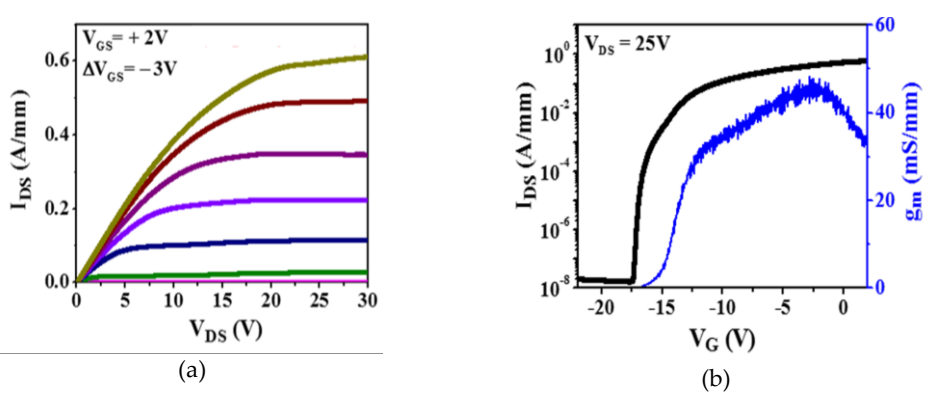


Fig. 9. EBG HEMT drain current ID (VD) (a), transfer ID (VG), and transconductance  $g_m$  (VG) (b) characteristics  $^{40}$ .

# 3. Discussion of the experimental results

The measured FBD value presents a low bound for the actual breakdown field value since the field distribution is non-uniform. Therefore, the breakdown occurs in the electric field peak forming at the contact metal edge. Our 2D simulations of the electric field profiles using Synopsys showed that the peak field is at least 15% higher than the average field (reaching approximately 13.1 MV/cm). This value is close to that estimated for the Al<sub>0.87</sub>GaN<sub>0.13</sub>N barrier material, and, as shown below, is expected for a QC HEMT design.

The breakdown field of the HEMT device can be estimated based on the composition of the device channel material. Using the Vegard's Law with the bandgaps of GaN E<sub>G1</sub> = 3.4 eV and AlN  $E_{G2}$  = 6.2 eV and bowing factor b=0.7  $^{63}$ , we obtain for the channel Al fraction x = 0.64

$$E_{GCH} = x E_{G2} + E_{G1} (1-x) - bx(1-x) = 5.03 \text{ eV},$$
 (4)

Next, using the bandgap-critical field relationship after 57

$$F_{CR} = 0.173 \ E_{G^{2.5}},$$
 (5)

we obtain  $F_{CR}$  = 9.8 MV/cm. As seen, the expected critical field is lower than the measured value. To explain this breakdown field increase, we involve the quantization effects in quantum channel devices. In QC-HEMT, the channel region forms a quantum well (QW), whose profile is mainly determined by the polarization charges at the top and bottom interfaces. Due to this, the QW maintains the triangular shape and, hence, supports strong confinement even at the gate bias below the threshold. In conventional HEMT, on the contrary, the Ec profile completely flattens out at gate bias close to V<sub>TH</sub>. The band diagrams of EBG QC-HEMT and conventional HEMT at different gate bias are compared in Fig. 2.

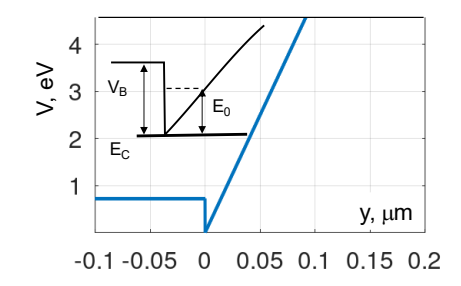


Fig. 10. Triangular QW profile used in MATLAB calculations of the ground state energy  $E_1$ . The barrier height at the Al<sub>0.87</sub>Ga<sub>0.13</sub>N/ Al<sub>0.64</sub>Ga<sub>0.36</sub>N barrier/channel interface,  $V_B$  = 0.72 eV, electric field in the channel  $F_{CH}$  = 0.5 MV/cm, electron effective mass in the channel,  $m_{EF}$  = 0.34  $m_0$ .

The average electric field in the QC HEMT channel estimated from the slope of the band diagram is  $F_{CH} \approx 0.5$  MV/cm. For an infinitely high triangular barrier, the lowest state energy is given by  $^{64}$ :

$$E_o = c_1 \left[ \frac{(qF_{CH}\hbar)^2}{2m_{EF}} \right]^{\frac{1}{3}} \tag{6}$$

where  $c_1$ =2.338, and  $m_{EF}$  is the effective electron mass in the channel. Using linear interpolation between GaN and AlN, we found  $m_{EF}$  = 0.34  $m_0$  for our 64%-Al AlGaN channel. The lowest energy level given by (6) is  $E_0$  = 0.16 eV above the conductance band edge EC.

The barrier/channel height calculated for our EBG HEMT composition is  $V_B = 0.72 \text{ eV}$ . Using MATLAB to find eigenvalues of the Schrodinger equation for a triangular QW with finite barrier height (see Fig. 13) yielded a more accurate value of  $E_0$ = 0.13 eV.

As illustrated in Fig. 10, the quantization in the channel results in a larger effective bandgap  $E_{GEF}$  than that corresponding to material composition:  $E_{GEF} = E_G + E_0 = 5.16$  eV (here we ignored quantization in the valence band). A higher  $E_{GEF}$  translates into a higher critical breakdown field evaluated as <sup>57</sup>.

$$F_{CR1} = 0.173 E_{GEF}^{2.5} = 10.46 \text{ MV/cm}$$
 (7)

The critical field accounting for the quantization effects in the QC-HEMT is closer to the measured value of 11.37 MV/cm but is still lower than that. Therefore, the quantization of energy states in the QC HEMT explains only a fraction of the excessive critical field observed in the experiment.

An additional important mechanism enhancing the breakdown field is the effect that we call the electron quantum real space transfer into the Al<sub>0.87</sub>Ga<sub>0.13</sub> barrier layer. As shown in <sup>5959</sup>, a larger density of states in quantum well cladding layers causes an increase of the wave function penetration into the cladding layers with an increase in the electron kinetic energy  $E_{kin}$  where k is the electron momentum in the channel plane. This transfer reduces the effective barrier height and completely eliminates the effective barrier for energetic electrons capable of causing impact ionization in the channel. The fraction of the remaining barrier height  $f_b$  is a function of the channel electrons kinetic energy  $E_{kin}$  to the barrier height  $V_B$  ratio: [<sup>29</sup>]

$$f_B = \sqrt{1 - E_0/V_B - E_{kin}/V_B (m_B/m_{EF} - 1)}$$
 (8)

Here  $m_B$  and  $m_{EFF}$  are the electron effective masses in the barrier and channel layers. In Fig. 11(a) we plotted the effective barrier reduction for the device parameters of our QC HEMT. As seen, the effective barrier disappears for electrons with  $E_{kin}/V_B \ge 4$ . Electrons causing impact ionization have kinetic energy  $E_{kin} > 6.2$  eV or  $E_{kin}/V_B > 8$ . Therefore, all very energetic electrons responsible for ionization should transfer into the

cladding layer and the expected breakdown field should be equal to the breakdown field in the cladding layer, in agreement with the measured breakdown field.



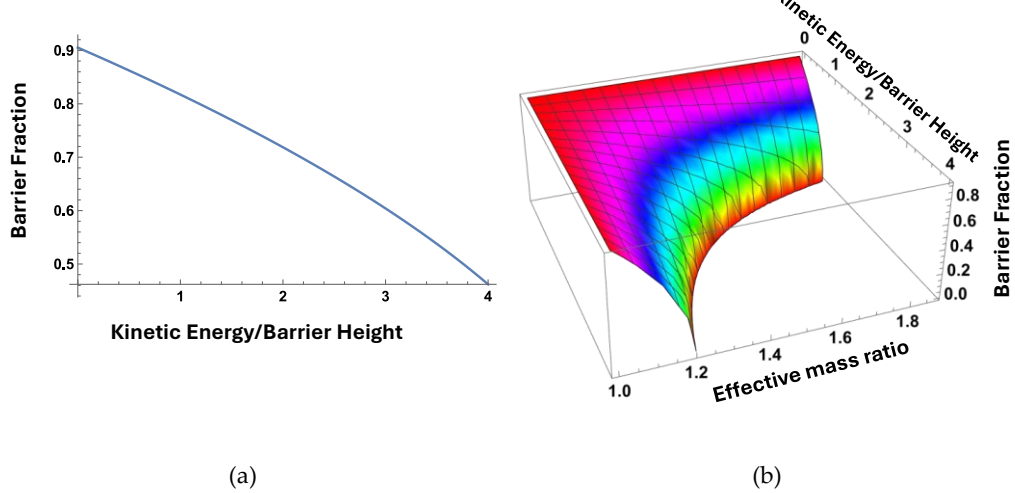


Fig. 11. Barrier reduction for energetic electrons: (a) effective barrier height versus kinetic energy of electrons for effective mass ratio in the QC HEMT studied in this paper and (b) effective barrier height versus kinetic energy of electrons for all mass ratios for AlN/GaN system.

Fig. 11(b) shows the barrier reduction as a function of both e1 and . The upper bound of the range of 1,87 corresponds to the effective mass ratio of AlN and GaN. As seen from the figure, a large difference in Al molar fraction between the barrier and the channel is beneficial for the quantum real transfer. Such designs having an additional advantage of having much higher electron mobility in the device channel could be achieved by making the channel thinner to avoid the development of the dislocation arrays.

It is interesting to compare the obtained breakdown field in EBG QC-HEMT device with other data available for conventional HEMTs and double-heterostructure HEMTs having epilayer structure similar to QC-HEMT. Numerous results have been published on breakdown in single heterostructure GaN- and AlGaN-channel HEMTs; vast majority of them report the breakdown fields, considerably lower than those expected from material parameters. One of the highest breakdown fields of 1.6 MV/cm have been achieved in Al<sub>0.15</sub>Ga<sub>0.75</sub>N HEMT <sup>65</sup>. As pointed out in <sup>66</sup> the breakdown fields achieved in double-heterostructure HEMTs are typically significantly (2 – 3 times) higher than those in single heterostructure devices. This observation is in agreement with the concept of QC-HEMT.

#### 2. Conclusions

In conclusion, the QC Extreme Bandgap AlGaN HEMT design demonstrated the possibility to considerably improve the breakdown voltage. QC HEMT approach also has a strong potential to increase field-effect mobility, and, therefore, transconductance at low electron sheet densities and support a large maximum electron sheet density and a larger maximum current. A thinner quantum well made of lower bandgap material should also lead to better radiation hardness of QC HEMT.

**Author Contributions:** Conceptualization, M. Shur and G. Simin; methodology, G. Simin, A. Khan, MVS Chandrashekhar; validation, K. Hussain, A. Mamun. All authors have read and agreed to the published version of the manuscript.

**Funding:** This research at USC was funded by Office of Naval Research (ONR) Multidisciplinary University Research Initiatives (MURI) contract ONR N00014-18-1-2033, Program Manager

M.	pt. L. Petersen, by Army Research Office contract W911NF-18-1-0029, Program Manager I Gerhold. The work at RPI and USC was supported by the Office of Naval Research grant "STEN Lantum Channel High Breakdown Voltage HEMT" N00014-23-1-2289-P00001 monitored by I
	Maki.
Da	ta Availability Statement: Data are contained within the article.
Con	<b>inflicts of Interest:</b> The authors declare no conflicts of interest.

**Disclaimer/Publisher's Note:** The statements, opinions and data contained in all publications are solely those of the individual author(s) and contributor(s) and not of MDPI and/or the editor(s). MDPI and/or the editor(s) disclaim responsibility for any injury to people or property resulting from any ideas, methods, instructions or products referred to in the content.

References 346

<sup>1</sup> M. A. Khan, J. N. Kuznia, D. T. Olson, W. Schaff, J. Burm, M. S. Shur, Microwave Performance of 0.25-micron Doped Channel GaN/AlGaN Heterostructure Field Effect Transistor, Appl. Phys. Lett, Vol. 65 (9), pp. 1121-1123 (1994)

- <sup>2</sup> Wu Y F, Keller B P, Keller S, Kapolnek D, Kozodoy P, Denbaars S P and Mishra U K (1996), Very high breakdownvoltage and large transconductance realized on GaN heterojunction field effect transistors Appl. Phys. Lett.69 1438–40
- <sup>3</sup> M. S. Shur and M. Asif Khan, AlGaN/GaN Doped Channel Heterostructure Field Effect Transistors, Physica Scripta, T69, 103-107 (1997)
- <sup>4</sup> Wu Y F, Chavarkar P M, Moore M, Parikh P, Keller B P and Mishra U K 2000 A 50-W AlGaN/GaN amplifier, Int. Electron Devices Meeting (San Francisco, CA, 2000)
- <sup>5</sup> S. Keller, Y. F. Wu, G. Parish, N. Ziang, J. J. Xu, B. P. Keller, S. P. DenBaars, and U. K. Mishra, Galliumnitride based high power heterojunction field effect transistors: process development and present status at UCSB, IEEE Trans. Elect. Dev. 48, 552 (2001)
- <sup>6</sup> H. Xing, et al, Gallium nitride based transistors, J. Phys: Condens. Matter 13 (2001) 7139, DOI 10.1088/0953-8984/13/32/317
- <sup>7</sup> W. Saito, Y. Takada, M. Kuraguchi, K. Tsuda, I. Omura, T. Ogura, and H. Ohashi, "High breakdown voltage AlGaN–GaN power-HEMT design and high current density switching behavior," IEEE Trans. Electron Devices, vol. 50, no. 12, pp. 2528–2531, Dec. 2003
- <sup>8</sup> N. Tipirneni, V. Adivarahan, G. Simin and A. Khan, Silicon Dioxide Encapsulated High Voltage AlGaN/GaN HFETs for Power Switching Applications, IEEE El. Dev. Lett. V. 28, 784-786 (2007)
- <sup>9</sup> Zhang, Y., Li, Y., Wang, J. et al. High-Performance AlGaN Double Channel HEMTs with Improved Drain Current Density and High Breakdown Voltage. Nanoscale Res Lett 15, 114 (2020). https://doi.org/10.1186/s11671-020-03345-6
- <sup>10</sup> Yang C, Luo X, Sun T, Zhang A, Ouyang D, Deng S, Wei J, Zhang B, High Breakdown Voltage and Low Dynamic ON-Resistance AlGaN/GaN HEMT with Fluorine Ion Implantation in SiNx Passivation Layer, (2019) Nanoscale Res Lett 14:191
- <sup>11</sup> P.-C. Chao, Chu, K. Creamer, C. Diaz, J. Yurovchak, T. Shur, M. Kallaher, R. McGray, C. Via, G.D. Blevins, J.D. Low-Temperature Bonded GaN-on-Diamond HEMTs with 11 W/mm Output Power at 10 GHz, IEEE Transactions on Electron Devices, Volume: 62, Issue: 11, Pages: 3658-3664, DOI: 10.1109/TED.2015.2480756 (2015)
- <sup>12</sup> Mishra U, Shen L, Kazior T, Wu Y. GaN-based RF power devices and amplifiers. Proc IEEE 2008;96:287–305
- <sup>13</sup> Baca AG, Klein BA, Wendt JR, Lepkowski SM, Nordquist CD, Armstrong AM, Allerman AA, Douglas EA, Kaplar RJ, RF Performance of Al0.85Ga0.15N/Al0.70Ga0.30N High Electron Mobility Transistors With 80-nm Gates, (2019) IEEE Electron Device Lett 40:17
- <sup>14</sup> Wu Y, Zhang J, Zhao S, Zhang W, Zhang Y, Duan X, Chen J, Hao Y, More Than 3000 V Reverse Blocking Schottky-Drain AlGaN-Channel HEMTs With >230 MW/cm2 Power Figure-of-Merit, (2019) IEEE Electron Device Lett 40:1724
- <sup>15</sup> Y.-F. Wu, B.P. Keller, P. Fini, J. Pusl, M. Le, N. X. Nguyen, C. Nguyen, D. Widman, S. Keller, S. P. Denbaars, and U. K. Mishra, Short-channel Al<sub>0.5</sub>Ga<sub>0.5</sub>N/GaN MODFETs with power density > 3 W/mm at 18 GHz Electron. Lett. 33 p. 1742 (1997)
- <sup>16</sup> Mishra U, Shen L, Kazior T, Wu Y. GaN-based RF power devices and amplifiers. Proc IEEE 2008;96:287–305
- <sup>17</sup> S. J. Pearton et al, Review Ionizing Radiation Damage Effects on GaN Devices
   2016 ECS J. Solid State Sci. Technol.
   5 Q35 DOI 10.1149/2.0251602jss

- <sup>18</sup> Sequeira, M. C., Mattei, J., Vazquez, H., Djurabekova, F., Nordlund, K., Monnet, I., Kluth, P., Grygiel, C., Zhang, S., Alves, E., & Lorenz, K. (2021). Unravelling the secrets of the resistance of GaN to strongly ionising radiation. Communications Physics, 4(1), 1-8. https://doi.org/10.1038/s42005-021-00550-2
- <sup>19</sup> A. Bykhovski, B. Gelmont, and M. S. Shur, The Influence of the Strain-Induced Electric Field on the Charge Distribution in GaN-AlN-GaN SIS Structure, J. Appl. Phys. Dec. Vol. 74 (11), p. 6734-6739 (1993)
- <sup>20</sup> O. Ambacher; B. Foutz; J. Smart; J. R. Shealy; N. G. Weimann; K. Chu; M. Murphy; A. J. Sierakowski; W. J. Schaff; L.
- F. Eastman; R. Dimitrov; A. Mitchell; M. Stutzmann, Two-dimensional electron gases induced by spontaneous and piezoelectric polarization in undoped and doped AlGaN/GaN heterostructures. J. Appl. Phys. 87, 334–344 (2000), https://doi.org/10.1063/1.371866
- <sup>21</sup> E. T. Yu, G. J. Sullivan, P. M. Asbeck, C. D. Wang, D. Qiao, and S. S. Lau, Measurement of piezoelectrically induced charge in GaN/AlGaN heterostructure field-effect transistors, Appl. Phys. Lett., 1997, 71, 2794–2796.
- <sup>22</sup> Rathore, S.U.; Dimitrijev, S.; Amini Moghadam, H.; Mohd-Yasin, F. Equations for the Electron Density of the Two-Dimensional Electron Gas in Realistic AlGaN/GaN Heterostructures. Nanomanufacturing 2021, 1, 171-175. https://doi.org/10.3390/nanomanufacturing1030012
- <sup>23</sup> M. E. Levinshtein, S. L. Rumyantsev, and M. S. Shur, Editors, "Properties of Advanced Semiconductor Materials: GaN, AlN, InN, BN, SiC, and SiGe", J. Wiley and Sons, ISBN 0-471-35827-4, New York (2001)
- <sup>24</sup> J.-Z. Zhang, A. Dyson, and B. K. Ridley, Momentum relaxation due to polar optical phonons in AlGaN/GaN heterostructures, Phys. Rev. B 84, 155310 Published 17 October 2011
- <sup>25</sup> Ahmed Mohamed ,Kihoon Park,Can Bayram,Mitra Dutta,Michael Stroscio, Confined and interface optical phonon emission in GaN/InGaN double barrier quantum well heterostructures, PLOS ONE 14(5): e0216630. April 18, 2019, https://doi.org/10.1371/journal.pone.0214971
- <sup>26</sup> M. E. Levinshtein, S. Rumyantsev, and M. S. Shur, Editors, Handbook of Semiconductor Material Parameters, Si, Ge, C (diamond), GaAs, GaP, GaSb, InAs, InP, InSb, Vol. 1, World Scientific, 1996, ISBN 981-02-2934-8517.
- <sup>27</sup> Fu, Z., Yamaguchi, M. Coherent Excitation of Optical Phonons in GaAs by Broadband Terahertz Pulses. Sci Rep 6, 38264 (2016). https://doi.org/10.1038/srep38264
- <sup>28</sup> Lockwood, D. J., Yu, G. L. & Rowell, N. L. Optical phonon frequencies and damping in AlAs, GaP, GaAs, InP, InAs and InSb studied by oblique incidence infrared spectroscopy. Solid State Commun. 136, 404–409 (2005).
- <sup>29</sup> P.A. Ivanov, M.E. Levinshtein, G. Simin, X. Hu, J. Yang, M. A. Khan, S. L. Rumyantsev, M. S. Shur and R. Gaska, Drift mobility of electrons in AlGaN/GaN MOSHFET, Electronics Letters, vol. 37 (24), pp. 1479-1481 (2001)
- <sup>30</sup> Alice Hospodková, František Hájek, Tomáš Hubáček, Zuzana Gedeonová, Pavel Hubík, Jiří J. Mareš, Jiří Pangrác, Filip Dominec, Karla Kuldová, Eduard Hulicius, Electron mobility in GaN layers and HEMT structure optimized by MOVPE technological parameters, Journal of Crystal Growth, Volume 605, 2023, 127061, https://doi.org/10.1016/j.jcrysgro.2022.127061.
- <sup>31</sup> Sung-Jae Chang et al, Investigation of channel mobility in AlGaN/GaN high-electron-mobility transistors, 2016 Jpn. J. Appl. Phys. 55 044104, DOI 10.7567/JJAP.55.044104
- <sup>32</sup> Y. Cordier, M. Hugues, P. Lorenzini, F. Semond, F. Natali, and J. Massies. Electron mobility and transfer characteristics in AlGaN/GaN, HEMTs, phys. stat. sol. (c) 2, No. 7, 2720–2723 (2005) / DOI 10.1002/pssc.200461470
- <sup>33</sup> Raymond S. Pengelly et. al.A Review of GaN on SiC High Electron-Mobility Power Transistors and MMICs, m IEEE Transactions on Microwave Theory and Techniques, VOL. 60, NO. 6, JUNE 2012
- Alice Hospodková et al. Electron Transport Properties in High Electron Mobility Transistor Structures Improved by V-Pit Formation on the AlGaN/GaN Interface ACS Applied Materials & Interfaces 2023 15 (15), 19646-19652

- <sup>35</sup> Hájek, F.; Hospodková, A.; Hubík, P.; Gedeonová, Z.; Hubáček, T.; Pangrác, J.; Kuldová, K. Transport Properties of AlGaN/GaN HEMT Structures with Back Barrier: Impact of Dislocation Density and Improved Design. Semicond. Sci. Technol. 2021, 36, 075016 DOI: 10.1088/1361-6641/abfe9b
- <sup>36</sup> E. Frayssinet, W. Knap, P. Lorenzini, N. Grandjean and J. Massies, C. Skierbiszewski, T. Suski, I. Grzegory, S. Porowski, G. Simin, X. Hu, M. A. Khan, M. Shur, R. Gaska, and D. Maude, High electron mobility in AlGaN/GaN heterostructures grown on bulk GaN substrates, Appl. Phys. Lett, Vol. 77, No. 16, pp. 2551-2553, October (2000)
- <sup>37</sup> R. Gaska, M. S. Shur, A. D. Bykhovski, A. O. Orlov, and G. L. Snider, Electron Mobility in Modulation Doped AlGaN-GaN Heterostructures, Appl. Phys. Lett. 74, No. 2, January 11, pp. 287-289 (1999)
- <sup>38</sup> A. Azimi, M. Azimi, M. S. Shur, and S. K. O'Leary. The impact of device length on the electron's effective mobility, J. App. Phys., 134, 125701 (2023), https://doi.org/10.1063/5.0171559
- <sup>39</sup> Hussain, Kamal, et al. "High figure of merit extreme bandgap Al<sub>0.87</sub>Ga<sub>0.13</sub>N-Al<sub>0.64</sub>Ga<sub>0.36</sub>N heterostructures over bulk AlN substrates." Applied Physics Express 16.1 (2023): 014005.
- <sup>40</sup> Mamun, Abdullah, et al. "Al<sub>0.64</sub> Ga<sub>0.36</sub>N channel MOSHFET on single crystal bulk AlN substrate." Applied Physics Express 16.6 (2023): 061001.
- <sup>41</sup> R. Gaska, C. Chen, J. Yang, E. Kuokstis, A. Khan, G. Tamulaitis, I. Yilmaz, M. S. Shur, J. C. Rojo, L. Schowalter, Deepultraviolet emission of AlGaN/AlN quantum wells on bulk AlN, Appl. Phys. Lett. Vol. 81, No 24, pp. 4658-4660, (2002)
- <sup>42</sup> J. Singhai et al. AlN/AlGaN/AlN quantum well channel HEMTs, Appl. Phys. Lett. 122, 222106 (2023), https://doi.org/10.1063/5.0145582
- <sup>43</sup> J. Y. Tsao et al. "Ultrawide-bandgap semiconductors: Research opportunities and challenges," Adv. Electron. Mater. 4, 1600501 (2018).https://doi.org/10.1002/aelm.201600501.
- <sup>44</sup> A. G. Baca, A. M. Armstrong, B. A. Klein, A. A. Allerman, E. A. Douglas, and R. J. Kaplar, "Al-rich AlGaN based transistors," J. Vacuum Sci. Technol. A: Vacuum, Surf., Films 38, 020803 (2020).https://doi.org/10.1116/1.5129803
- R. J. Kaplar, A. A. Allerman, A. M. Armstrong, M. H. Crawford, J. R. Dickerson, A. J. Fischer, A. G. Baca, and E. A. Douglas, "Review—Ultra-wide-bandgap AlGaN power electronic devices," ECS J. Solid State Sci. Technol. 6, Q3061–Q3066 (2017).https://doi.org/10.1149/2.0111702jss
- <sup>46</sup> Yu-Hsin Chen et al., High conductivity coherently strained quantum well XHEMT heterostructures on AlN substrates with delta doping, Appl. Phys. Lett. 125, 142110 (2024), https://doi.org/10.1063/5.0228253.
- <sup>47</sup> G. Li, R. Wang, J. Guo, J. Verma, Z. Hu, Y. Yue, F. Faria, Y. Cao, M. Kelly, T. Kosel et al., "Ultrathin body GaN-on-insulator quantum well FETs with regrown Ohmic contacts," IEEE Electron Device Lett. 33, 661–663 (2012).
- <sup>48</sup> X. Hu, J. Deng, N. Pala, R. Gaska, M. S. Shur, C. Q. Chen, J. Yang, S. Simin, and A. Khan, C. Rojo, L. Schowalter, AlGaN/GaN Heterostructure Field Effect Transistor on Single Crystal Bulk AlN, Appl. Phys. Lett, 82, No 8, pp. 1299-1302, 24 Feb (2003)
- <sup>49</sup> G. Tamulaitis, I. Yilmaz, M. S. Shur, R. Gaska, C. Chen, J. Yang, E. Kuokstis, A. Khan, S.B. Schujman, L. J. Schowalter, Photoluminescence of GaN Deposited on Single Crystal Bulk AlN with Different Polarities, Appl. Phys. Lett. 83, No 17, pp. 3507-3509 (2003)
- <sup>50</sup> J. R. Grandusky et al. Manufacturability of high power ultraviolet-C light emitting diodes on bulk aluminum nitride substrates, Solid State Electron. December 2012, Pages 127-130.
- <sup>51</sup> T. Nagashima et al. Homoepitaxial growth of AlN on a 2-in.-diameter AlN single crystal substrate by hydride vapor phase epitaxy. Volume 540, 15 June 2020, 125644
- <sup>52</sup> X. Yao et al, State-of-the-art and prospective progress of growing AlN substrates by physical vapor transport, Journal of Crystal Growth, Volume 617, 1 September 2023, 127276https://doi.org/10.1016/j.jcrysgro.2023.127276

- <sup>53</sup> S. Xiao et al. Thick AlN layers grown on micro-scale patterned sapphire substrates with sputter-deposited annealed AlN films by hydride vapor-phase epitaxy, J. Cryst. Growth Volumes 566–567, 15 July 2021, 126163
- <sup>54</sup> G. Snider, 1D Poisson a program for calculating energy band diagrams for semiconductor structures. https://www3.nd.edu/~gsnider/, accessed October 10, 2023
- 55 L. D. Landau, L. M. Lifshitz, Quantum Mechanics: Non-Relativistic Theory, 3rd Edition, Elsevior
- <sup>56</sup> M. S. Shur, Introduction to Electronic Devices, J. Wiley and Sons, New York, 1996, ISBN 0-471-10348-9, ISBN 981-02-2325
- <sup>57</sup> J. L. Hudgins, G.S. Simin, E. Santi, M. Asif Khan, An Assessment of Wide bandgap Semiconductors for Power Devices, IEEE Trans. on Power Electronics, V.18, 907-914 (2003)
- <sup>58</sup> W. A. Hadi, M. S. Shur, and S. K. O'Leary Review: Steady-state and transient electron transport within the wide energy gap compound semiconductors gallium nitride and zinc oxide: An updated and critical review, Journal of Materials Science: Materials in Electronics, J Mater Sci: Mater Electron (2014) 25:4675–4713 DOI 10.1007/s10854-014-2226-2
- <sup>59</sup> M. Dyakonov and M. S. Shur, Consequences of space dependence of effective mass in heterostructures, J. Appl. Phys, V 84, N7, p. 3726 (1998)
- <sup>60</sup> C. Chen, J. Zhang, V. Adivarahan, A. Koudymov, H. Fatima, G. Simin, J. Yang, and M. Asif Khan, AlGaN/GaN/AlGaN Double Heterostructure for high power III-N FETs, Appl. Phys. Lett. 82, 4593 (2003)
- <sup>61</sup> J. Khurgin, S. Bajaj and S. Rajan, Amplified spontaneous emission of phonons as a likely mechanism for density-dependent velocity saturation in GaN transistors, Applied Physics Express 9, 094101, 2016
- <sup>62</sup> S. Rajan, S. DenBaars, U. Mishra, H. Xing, and D Jena, Electron mobility in graded AlGaN alloys, Applied Physics Letters 88, 042103 (2006)
- 63 F. Yun et. al. Energy band bowing parameter in AlxGa1-xN alloys Appl. Phys. 92, 4837 (2002)
- 64 J. Davies, The Physics of Low-Dimensional Semiconductors, Cambridge University Press (1998)
- 65 T. Nanjo et. al, AlGaN Channel HEMT With Extremely High Breakdown Voltage, IEEE Trans. El. Dev., 60, 1046 (2013)
- <sup>66</sup> Gaudenzio Meneghesso, Matteo Meneghini, and Enrico Zanoni, Breakdown mechanisms in AlGaN/GaN HEMTs: An overview, Jap. Journ. Appl. Phys, 53, 100211 (2014)